(Received 13 December 2024, Accepted 15 January 2025, Scheduled 26 January 2025)

Maximally Flat Negative Group Delay Prototype Filter Based on Capped Reciprocal Transfer Function of Classical Bessel Filter

Miodrag Kandic[1, 2, *] and Greg E. Bridges[1, 3]

[1] *Department of Electrical and Computer Engineering University of Manitoba, Winnipeg, Manitoba, Canada*
[2] *ORCID: 0000-0002-3673-4706*
[3] *ORCID: 0000-0001-8147-9882*

ABSTRACT: A prototype filter design exhibiting Negative Group Delay (NGD) is presented, based on the ratio of two low-pass classical Bessel filter transfer functions of the same order, but with different 3 dB-bandwidths. The resulting design is a reciprocal-Bessel filter transfer function, capped at a finite out-of-band gain. The proposed capped reciprocal-Bessel design is based on a similar concept applied to previously reported capped reciprocal-Butterworth and reciprocal-Chebyshev NGD designs, which use ratios of corresponding classical low-pass filter transfer functions. It is shown that within the in-band frequency range, the synthesized NGD transfer function exhibits a maximally flat group delay characteristic (Bessel-like property). Due to its near-flat in-band group delay characteristic, the design is suitable for constant phase shifter applications. For high design orders, it is shown that the achieved NGD-bandwidth product has an upper asymptotic limit, given by the square root of the out-of-band gain in decibels. When the prototype baseband transfer function is translated to a non-zero center frequency, it is demonstrated that resonator-based implementations are feasible via Sallen-Key, as well as all-passive ladder topologies. A combined in-band magnitude/phase distortion metric is evaluated for selected design examples and applied Gaussian and sinc input waveforms, and it is shown to be proportional to the design order and out-of-band gain. The proposed design's distortion metric is also shown to be generally lower than the previously reported capped reciprocal-Butterworth and reciprocal-Chebyshev designs.

1. INTRODUCTION

Negative group delay (NGD) phenomenon is an example of abnormal wave propagation, in addition to superluminal [1], negative refractive index [2], simultaneous negative phase and group velocity [3], and others. NGD is observed in anomalous dispersion media and circuits which exhibit a positive phase characteristic slope within a finite frequency band. Time domain waveforms with their frequency spectrums mostly contained within a finite NGD band get reshaped by the medium, such that distinct parts of the output waveform (peak of a pulse for example) are temporally advanced relative to the input waveform. Such seemingly counter-intuitive phenomenon does not violate causality, since any non-analytical part of the waveform (such as "front", or onset) is still positively delayed and propagates at a subluminal velocity [4–6].

Utilizing Kramers-Kronig relations between magnitude and phase characteristics in causal linear media, it was shown that the magnitude response has a minimum within a frequency band exhibiting NGD [7]. Accordingly, maximum signal attenuation (SA) is present within an NGD bandwidth of gain-uncompensated designs. The SA is corrected in gain-compensated designs, although an out-of-band gain gets introduced as well. Therefore, a relative out-of-band to in-band gain is observed in both types of NGD designs. Out-of-band gain is a trade-off quantity accompanying NGD phenomenon, and is shown to be proportional to undesired amplification of the output transients associated with waveform discontinuities, such as finite "turn on/off" points in time [8–11]. Further, it was shown that a prominent transient response can be caused by medium's out-of-band gain at any non-analytical points, including discontinuities in waveform derivatives [12].

The NGD-bandwidth product's trade-off relationship with the maximum out-of-band gain was functionally quantified for selected media in [8–10, 13, 14]. For example, in the upper asymptotic limit the NGD-bandwidth product was shown to have a square root relationship with the maximum out-of-band gain given in decibels for a distributed medium with cascaded identical 1st-order baseband, or identical non-zero center frequency 2nd-order NGD circuits [8]. A similar square root asymptotic relationship, but with a higher proportionality factor, was derived for an engineered causal medium with a chosen flat in-band NGD characteristic and its magnitude characteristic obtained via Kramers-Kronig relations [9]. A power of 3/4 asymptotic relationship was shown for a distributed medium with cascaded identical 2nd-order baseband NGD circuits [10]. A generalization of the trend associated with cascaded identical Nth-order baseband NGD circuits was demonstrated in the capped reciprocal-Butterworth design presented in [13], with the NGD-bandwidth product shown to be proportional to the decibel value of the maximum out-of-band gain raised to the power of $(1 - 1/2N)$. Further, for a single stage of the Nth-order capped reciprocal-Butterworth design, the upper asymp-

* Corresponding author: Miodrag Kandic (Miodrag.Kandic@umanitoba.ca/ kandic@ngdfilters.com).

totic NGD-bandwidth product limit was shown to be a linear function of the maximum out-of-band gain in decibels [13]. An Nth-order capped reciprocal-Chebyshev NGD filter design was introduced in [14], exhibiting a higher NGD-bandwidth product relative to the capped reciprocal-Butterworth design for the same maximum out-of-band gain and the same design order, but at the expense of somewhat increased amplitude/phase distortion. The upper asymptotic NGD-bandwidth product limit was shown to be the same linear function associated with the capped reciprocal-Butterworth design, increased by an offset term.

In this paper, a similar NGD transfer function synthesis concept presented in [13, 14] for designs based on classical Butterworth and Chebyshev filters is applied to the classical Bessel filter design. The reciprocal transfer function of a low-pass Bessel filter is multiplied by another low-pass Bessel filter transfer function with the same order but with a larger bandwidth, resulting in a capped out-of-band gain of the overall transfer function which makes the design implementation practically possible. It is shown that such synthesized capped reciprocal-Bessel transfer function, when translated from baseband to its higher center frequency equivalent, can be implemented with resonator-based designs in Sallen-Key, and all-passive ladder topologies.

For a capped reciprocal-Bessel design, it is shown that as the order approaches infinity the achieved NGD-bandwidth product has an upper asymptotic limit that is the same square root function of out-of-band gain in decibels as that associated with a distributed medium with cascaded identical 1st-order baseband NGD stages [8, 13], but with a higher proportionality factor. This proportional factor of the square root asymptotic function is close to that of the engineered flat in-band NGD characteristic causal medium presented in [9], as expected given the group delay flatness property of the capped reciprocal-Bessel design presented here.

An in-band combined magnitude/phase distortion metric discussed in [15, 16] and modified as in [10, 13, 14] is evaluated for the proposed capped reciprocal-Bessel design and selected input waveforms. The proposed design is shown to exhibit a lower distortion than corresponding capped reciprocal-Butterworth [13] and capped reciprocal-Chebyshev [14] designs for the same design order and out-of-band gain, due to its very flat in-band group delay (linear phase) within the 3 dB-bandwidth. As a tradeoff, the proposed capped reciprocal-Bessel design exhibits a smaller NGD-bandwidth product than the other two. The very flat in-band group delay makes the proposed capped reciprocal-Bessel transfer function suitable for constant phase shifter implementations [17, 18], which are used in phased array antenna applications.

NGD designs, such as those in [8, 19–38], are commonly compared based on achieved NGD-bandwidth product and relative out-of-band gain metrics. NGD designs in this paper and those in [13, 14] are compared using the same metrics, as well as for the in-band magnitude/phase performance metric presented in [13, 14] to provide a measure of waveform distortion. An alternative in-band magnitude/phase distortion metric is presented in [39].

2. PROTOTYPE NGD FILTER BASED ON CAPPED RECIPROCAL LOW-PASS BESSEL FILTER TRANSFER FUNCTION

Example NGD designs based on 1st and 2nd-order baseband rational transfer functions were presented in [9, 10, 19, 40, 41], and a design with non-integer power functions was presented in [42]. An NGD design based on capped reciprocal-Butterworth filter transfer functions exhibiting a near-flat in-band magnitude response was reported in [13], while a capped reciprocal-Chebyshev design exhibiting a higher NGD-bandwidth product but with a ripple in the in-band magnitude and group delay responses was reported in [14].

Extending the transfer function synthesis concept presented for capped reciprocal-Butterworth [13, 43] and capped reciprocal-Chebyshev [14, 43] designs, a capped reciprocal-Bessel NGD transfer function can be obtained by taking a ratio of two Nth-order low-pass Bessel filter transfer functions with different 3 dB-bandwidths:

$$H\left(j\omega\right) = H_{reciprocal-LP}\left(j\omega\right) \cdot H_{capping-LP}\left(j\omega\right)$$

$$= \frac{1}{H_{LP-Bessel}\left(j\frac{\omega}{\omega_{c1}}\right)} \cdot H_{LP-Bessel}\left(j\frac{\omega}{\omega_{c2}}\right). \quad (1)$$

For the NGD to exist, according to [7] the magnitude of the transfer function (1) needs to have a minimum around the center frequency, which translates into the capping function having a higher 3 dB-bandwidth than the reciprocal function, $\omega_{c2} > \omega_{c1}$. The design process is described in a patent application [44]. The magnitude responses of a capped reciprocal-Bessel design transfer function (1) and its reciprocal and capping parts are illustrated in Fig. 1(a), showing a finite out-of-band gain, A. Similarly, Fig. 1(b) illustrates a near-flat NGD in-band response of (1), which is a signature property of the proposed design. Transfer function (1) can also be scaled by $1/A$ to represent its gain-uncompensated version, which doesn't affect its group delay characteristic.

The term producing the NGD in (1) is a reciprocal function of a Bessel low-pass filter transfer function, $1/H_{LP-Bessel}(j\omega/\omega_{c1})$, but this term alone would exhibit an infinite out-of-band gain. Therefore, to make the design feasible an out-of-band gain "capping" is needed and realized by the multiplying low-pass Bessel transfer function, $H_{LP-Bessel}(j\omega/\omega_{c2})$, as depicted in (1). Further, it can be shown that the bandwidth ratio of the reciprocal and capping functions needs to be $\omega_{c2}/\omega_{c1} = A^{1/N}$, to yield an out-of-band gain A of the overall Nth-order capped reciprocal-Bessel transfer function.

The denominator polynomial of the overall transfer function in (1) emerges from the capping function, which corresponds to the classical low-pass Bessel filter transfer function. Therefore, the overall transfer function in (1) has poles in the $s = j\omega$ complex Left Half-Plane (LHP) and is inherently stable.

From expression (1), the proposed Nth-order capped reciprocal-Bessel design baseband transfer function is given

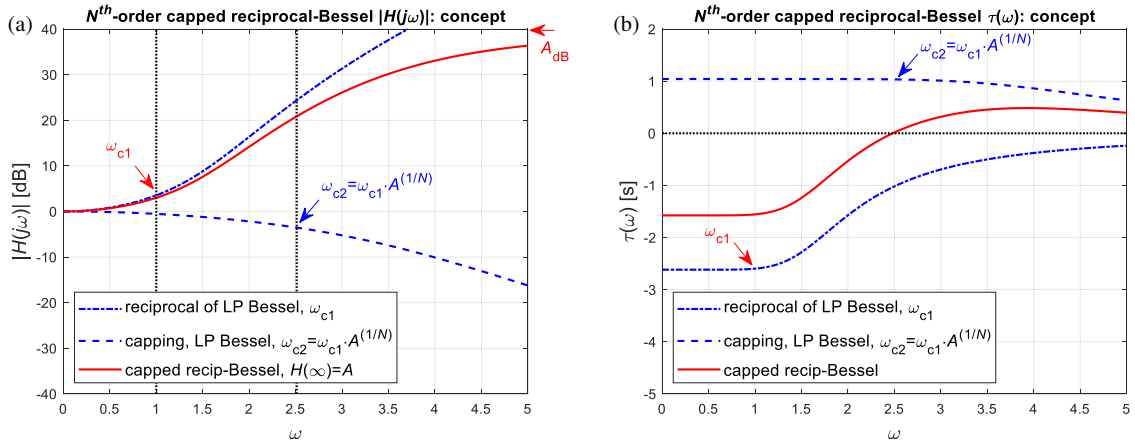

FIGURE 1. Example 5th-order capped reciprocal-Bessel NGD baseband design, out-of-band gain $A = 100$ ($A_{\text{dB}} = 40\,\text{dB}$), $N = 5$, capping to reciprocal transfer function 3 dB cut-off frequency ratio $\omega_{c2}/\omega_{c1} = A^{(1/N)} = 2.512$.

by:

$$H_N(j\omega') = \frac{\begin{array}{c} a_0 + a_1(j\omega') + a_2(j\omega')^2 \\ +\ldots + a_N(j\omega')^N \end{array}}{\begin{array}{c} a_0 + a_1\left(\frac{j\omega'}{A^{1/N}}\right) + a_2\left(\frac{j\omega'}{A^{1/N}}\right)^2 \\ +\ldots + a_N\left(\frac{j\omega'}{A^{1/N}}\right)^N \end{array}}, \tag{2a}$$

where the numerator and denominator parameters are as in Nth-order low-pass Bessel filter:

$$a_k = \frac{(2N-k)!}{2^{N-k}k!\,(N-k)!}, \tag{2b}$$

for $k = 0, 1, \ldots, N$, and the normalized frequency ω' represents frequency ω scaled by a 3 dB cut-off frequency correction factor, given by:

$$\omega' = \frac{\omega}{C_{\omega-3\,\text{dB}}}. \tag{2c}$$

The correction factor needs to be numerically estimated for accurate results, with some example values shown in Table 1. This correction factor can be approximated for large value of the design order, N, by an expression derived later in this paper:

$$C_{\omega-3\,\text{dB}} \approx \sqrt{\frac{1-1/A^{2/N}}{(2N-1)\ln 2}}, \quad N \gg 1. \tag{2d}$$

TABLE 1. Numerically determined values of the 3 dB cut-off frequency correction factor, $C_{\omega-3\,\text{dB}}$, for selected capped reciprocal-Bessel design orders $N = 2, 3, 4, 5$ and out-of-band gains $A = 10, 20, 30, 40$ dB.

	$N=2$	$N=3$	$N=4$	$N=5$
$A = 10\,\text{dB}$	1/1.654	1/2.288	1/2.956	1/3.642
$A = 20\,\text{dB}$	1/1.43	1/1.938	1/2.469	1/3.007
$A = 30\,\text{dB}$	1/1.382	1/1.833	1/2.293	1/2.75
$A = 40\,\text{dB}$	1/1.368	1/1.79	1/2.209	1/2.617

As a correction factor numerical example, for out-of-band gain $A = 100$ (40 dB), the 3 dB cut-off frequency correction factors for orders $N = 2, 5$ yield $C_{\omega-3\,\text{dB}} = 0.731, 0.3821$, whereas approximation (2d) yields 0.69 and 0.3673, respectively (5.6% and 3.9% error, respectively).

From expressions (2a)–(2c), example capped reciprocal-Bessel transfer functions for designs with orders $N = 2, 3, 5$, scaled for 3 dB-bandwidth at $\omega_c = 1$, and for given out-of-band gain $A = 100$ (40 dB), are given by:

$$\begin{aligned} H_{2nd}(j\omega) &= A\frac{3 + 3(j\omega') + (j\omega')^2}{3A + 3A^{1/2}(j\omega') + (j\omega')^2} \\ &= 100\frac{\omega^2 - j2.193\omega - 1.2661^2}{\omega^2 - j21.93\omega - 12.661^2}, \end{aligned} \tag{3a}$$

$$\begin{aligned} H_{3rd}(j\omega) &= 100\left(\frac{\omega - j\cdot 1.2973}{\omega - j\cdot 6.0216}\right) \\ &\quad\cdot\left(\frac{\omega^2 - j\cdot 2.0546\omega - 1.4199^2}{\omega^2 - j\cdot 9.5368\omega - 6.5904^2}\right), \end{aligned} \tag{3b}$$

$$\begin{aligned} H_{5th}(j\omega) &= 100\left(\frac{\omega - j\cdot 1.3935}{\omega - j\cdot 3.5003}\right) \\ &\quad\cdot\left(\frac{\omega^2 - j\cdot 1.7766\omega - 1.6282^2}{\omega^2 - j\cdot 4.4626\omega - 4.0899^2}\right) \\ &\quad\cdot\left(\frac{\omega^2 - j\cdot 2.5617\omega - 1.4436^2}{\omega^2 - j\cdot 6.4346\omega - 3.6262^2}\right). \end{aligned} \tag{3c}$$

The gain-compensated designs from expression (2a) and correspondingly (3a)–(3c) can be divided by the out-of-band gain A, to get gain-uncompensated versions with the same group delay responses. Resulting magnitude plots are shown in Fig. 2(a) for several different design orders, and in Fig. 3(a) for several different relative out-of-band gains (center frequency attenuations). Figs. 2(b) and 3(b) show the corresponding group delay plots, demonstrating that the center frequency NGD increases with the design order, as well as with the out of band gain, respectively.

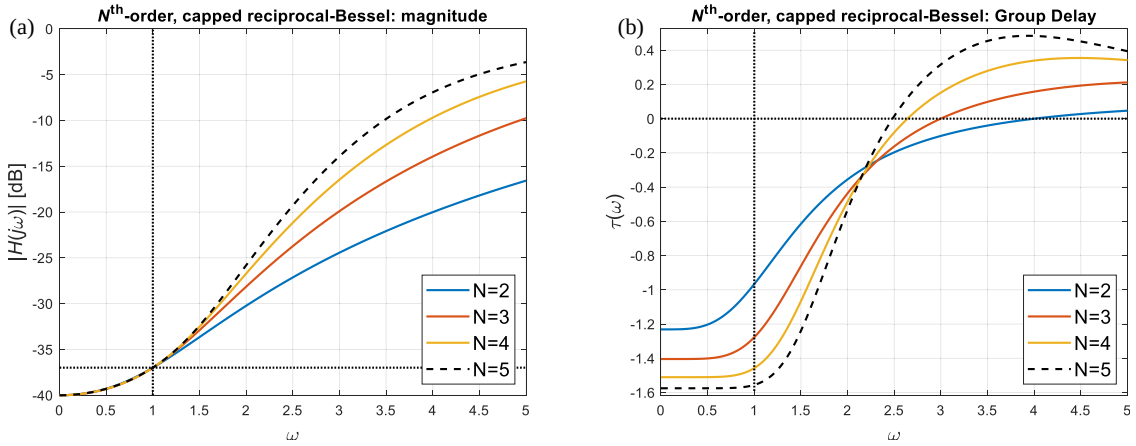

FIGURE 2. Proposed capped reciprocal-Bessel baseband transfer function NGD design with out-of-band gain $A = 100$ (40 dB), and $N = 2, 3, 4, 5$ order, (a) magnitude and (b) group delay plots.

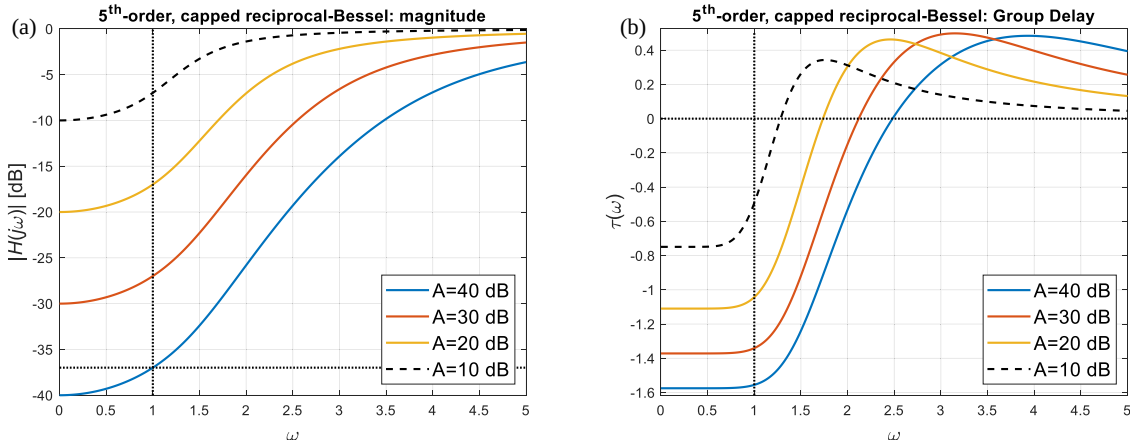

FIGURE 3. Proposed capped reciprocal-Bessel baseband 5th-order design with out-of-band gains $A = 10$ dB, 20 dB, 30 dB, 40 dB, (a) magnitude and (b) group delay plots.

The center frequency group delay value for a classical prototype low-pass Bessel filter transfer function without 3 dB-bandwidth scaling is equal to 1. Therefore, with accounting for frequency scaling in (2a) and (2c), the capped reciprocal-Bessel design center frequency NGD corrected for 3 dB-bandwidth at $\omega_c = 1$ is given by:

$$\tau(0) = -\frac{1}{C_{\omega-3\,\mathrm{dB}}}\left(1 - \frac{1}{A^{1/N}}\right). \tag{4}$$

In Fig. 2(b) examples with $A = 100$ (40 dB), expression (4) yields center frequency NGD values, NGD $= -\tau(0) =$ 1.2312 s, 1.4044 s, 1.5105 s, 1.5752 s for $N = 2, 3, 4, 5$, respectively. Since the corrected 3 dB-bandwidth cut-off frequency is $\omega_c = 1$, corresponding NGD-bandwidth product values are NGD $\cdot \Delta f$ = NGD $\cdot \omega_c/\pi = 0.3919$, 0.4470, 0.4808, 0.5014, for $N = 2, 3, 4, 5$, respectively. As a comparison, for the same $A = 100$ (40 dB) out-of-band gain, capped reciprocal-Butterworth design [13] yields larger values of NGD $\cdot \Delta f =$ 0.4052, 0.4995, 0.5688, 0.6200, for $N = 2, 3, 4, 5$, respectively, but at the expense of a large in-band group delay variation.

A similar NGD filter synthesis concept of using a classic low-pass filter reciprocal transfer function and capping it at a finite out-of-band gain by another low-pass transfer function with a wider bandwidth can also be applied to low-pass Pascal filters presented in [45]. Section 8 provides examples and compares capped reciprocal-Pascal, capped reciprocal-Butterworth [13] and capped reciprocal-Chebyshev [14] designs with the proposed capped reciprocal-Bessel design.

3. BASEBAND NGD FILTER TRANSFORMATION TO BAND-STOP-FILTER (BSF)

The baseband form of the proposed capped reciprocal-Bessel transfer function given by (2a) can be transformed into its non-zero center frequency, BSF equivalent. The general frequency variable substitution that achieves a transfer function transformation from baseband to its equivalent centered around ω_0, is given by [13]:

$$\omega \to \frac{1}{2}\left(\omega - \frac{\omega_0^2}{\omega}\right). \tag{5}$$

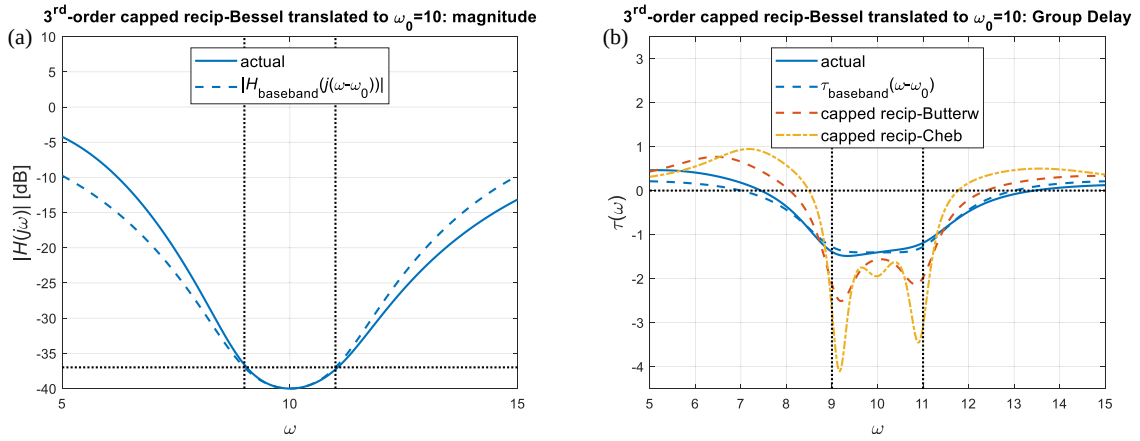

FIGURE 4. Example 3rd-order capped reciprocal-Bessel transfer function (a) magnitude and (b) group delay responses transformed to $\omega_0 = 10\omega_c = 10$ center frequency and compared with corresponding ideally translated baseband responses, as well as with group delays of capped reciprocal-Butterworth and capped reciprocal-Chebyshev (with a 0.5 dB in-band ripple) designs.

Applying transformation (5) to factorized 2nd-order baseband rational function(s) such as those appearing in (3a)–(3c), and captured in its general form (6a), yields an ω_0-centered BSF form given by (6b):

$$H_{BB2}(j\omega) = \left(\frac{\omega^2 - j\Delta\omega_1\omega - \omega_{01}^2}{\omega^2 - j\Delta\omega_2\omega - \omega_{02}^2}\right), \tag{6a}$$

$$H_{BSF2}(j\omega) = \left(\frac{\omega^2 - j\Delta\omega_{1p}\omega - \omega_{01p}^2}{\omega^2 - j\Delta\omega_{2p}\omega - \omega_{02p}^2}\right) \cdot \left(\frac{\omega^2 - j\Delta\omega_{3p}\omega - \omega_{03p}^2}{\omega^2 - j\Delta\omega_{4p}\omega - \omega_{04p}^2}\right). \tag{6b}$$

The factorized form of a BSF transfer function, as shown in (6b), is preferred to its expanded form since it is more suitable for subsequent circuit design [10, 13]. Expressions reported in [10] can be used to calculate the eight frequency parameters in (6b) from the four parameters in the baseband expression (6a). Several selected relationships between parameters in (6b) are given by [10, 13]:

$$\omega_{03p} = \frac{\omega_0^2}{\omega_{01p}}, \quad \Delta\omega_{3p} = \frac{\omega_0^2}{\omega_{01p}^2}\Delta\omega_{1p} = \frac{\omega_{03p}}{\omega_{01p}}\Delta\omega_{1p}, \tag{7}$$

showing that the BSF center frequency, ω_0, is the geometric mean of the transfer function numerator parameters ω_{01p} and ω_{03p}. Further, the quality factors of the two 2nd-order numerator functions are the same, $\omega_{01p}/\Delta\omega_{1p} = \omega_{03p}/\Delta\omega_{3p}$. Similar relationships apply to denominator parameters in (6b), as discussed in [10, 13].

Applying transformation (5) to factorized 1st-order baseband rational function(s) such as those appearing in (3b)–(3c) and captured in its general form (8a) yields an ω_0-centered BSF form given by (8b):

$$H_{BB1}(j\omega) = \left(\frac{\omega - j\Delta\omega_5}{\omega - j\Delta\omega_6}\right), \tag{8a}$$

$$H_{BSF1}(j\omega) = \frac{\omega^2 - j\Delta\omega_{5p}\omega - \omega_0^2}{\omega^2 - j\Delta\omega_{6p}\omega - \omega_0^2}, \tag{8b}$$

where $\Delta\omega_{5p} = 2\Delta\omega_5$ and $\Delta\omega_{6p} = 2\Delta\omega_6$.

As an example, a 3rd-order capped reciprocal-Bessel baseband transfer function given by (3b) is considered, with an $A = 100$ (40 dB) out-of-band gain. The gain-uncompensated version (divided by A) of this baseband transfer function yields:

$$H_{BB3}(j\omega) = \left(\frac{\omega - j\cdot 1.2973}{\omega - j\cdot 6.0216}\right) \cdot \left(\frac{\omega^2 - j\cdot 2.0546\omega - 1.4199^2}{\omega^2 - j\cdot 9.5368\omega - 6.5904^2}\right). \tag{9}$$

Employing frequency transformation (5), the BSF equivalent of this function centered around chosen $\omega_0 = 10\omega_c = 10$, after factorization into 2nd-order rational functions yields:

$$H_{BSF3}(j\omega) = \frac{\omega^2 - j2.5946\omega - 10^2}{\omega^2 - j12.0432\omega - 10^2} \cdot \left(\frac{\omega^2 - j2.2561\omega - 11.0338^2}{\omega^2 - j13.8211\omega - 16.2214^2}\right) \cdot \left(\frac{\omega^2 - j1.8531\omega - 9.0631^2}{\omega^2 - j5.2525\omega - 6.1647^2}\right). \tag{10}$$

The magnitude and group delay characteristics of ω_0-centered BSF transfer function (10) are shown in Figs. 4(a) and (b) plots, respectively.

A center frequency NGD of 1.4041 s is achieved by transfer function (10), or an NGD-bandwidth product of NGD $\cdot \Delta f = 0.447$ (virtually the same as its baseband equivalent). A relatively close in-band match is observed between the frequency characteristics associated with (10) and the corresponding ideally shifted baseband ones (expression (9) with $\omega \to \omega - \omega_0$). The near-flat baseband group delay characteristic has some slope in its ω_0-centered BSF equivalent, as evident from

Fig. 4(b). More deviation in the ω_0-centered group delay characteristic than magnitude characteristic is a consequence of a first derivative applied to the non-linear transformation (5) that accompanies group delay calculation. However, the in-band variation in the ω_0-centered group delay characteristic of the capped reciprocal-Bessel design presented in this paper is still lower than the corresponding capped reciprocal-Butterworth design from [13], and the capped reciprocal-Chebyshev 0.5 dB-ripple design from [14], as shown in Fig. 4(b). The very flat in-band group delay makes the proposed capped reciprocal-Bessel transfer function suitable for constant phase shifter implementations [17, 18], which are used in phased array antenna applications.

4. EXACT IMPLEMENTATION WITH SALLEN-KEY TOPOLOGY

An overall 6th-order BSF transfer function such as the one given by (10), obtained by upshifting a 3rd-order baseband capped reciprocal-Bessel transfer function to a non-zero center frequency ω_0, can be implemented by a Sallen-Key topology depicted in the Fig. 5 schematic. Similar to capped reciprocal-Butterworth and reciprocal-Chebyshev designs detailed in [13] and [14], respectively, higher order designs can be achieved with cascaded versions of the topology in Fig. 5. Transfer function of the topology in Fig. 5, and the input impedance of the design are given by, respectively [13]:

$$H(j\omega) = \frac{V_{out}}{V_{in}} = \frac{R_G \cdot R_F}{R_G \cdot R_F + Z_1 \cdot Z_2 + R_F \cdot (Z_1 + Z_2)} \frac{Z_0}{Z_0 + Z_3}, \quad (11)$$

$$Z_{in} = \frac{R_G \cdot R_F + Z_1 \cdot Z_2 + R_F \cdot (Z_1 + Z_2)}{R_F + Z_2}, \quad (12)$$

where Z_0 denotes the system impedance. As an implementation example, transfer function (11) associated with the Sallen-Key topology in Fig. 5 is equated to a particular capped reciprocal-Bessel transfer function given by (10), with its eight frequency parameters summarized as:

$$\begin{aligned} \omega_{01p} &= 11.0338\omega_c, \quad \Delta\omega_{1p} = 2.2561\omega_c, \\ \omega_{03p} &= 9.0631\omega_c, \quad \Delta\omega_{3p} = 1.8531\omega_c, \\ \omega_{02p} &= 16.2214\omega_c, \quad \Delta\omega_{2p} = 13.8211\omega_c, \end{aligned} \quad (13a)$$

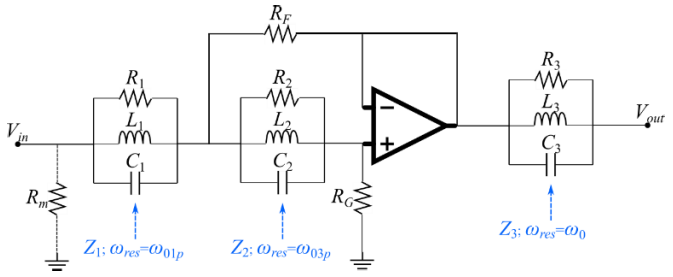

FIGURE 5. Sallen-Key topology that can be used to achieve an exact 3rd-order capped reciprocal-Bessel baseband NGD transfer function translated to a higher center frequency ω_0 (BSF).

$$\begin{aligned} \omega_{04p} &= 6.1647\omega_c, \quad \Delta\omega_{4p} = 5.2525\omega_c, \quad (13b) \\ \omega_0 &= 10\omega_c, \quad \Delta\omega_{5p} = 2.5946\omega_c, \\ \Delta\omega_{6p} &= 12.0432\omega_c. \quad (13c) \end{aligned}$$

Assuming a bandwidth of $\Delta f = 2f_c = 100$ MHz in the normalized expression (10), the center frequency becomes $f_0 = 10f_c = 500$ MHz. Further selecting the input impedance at center frequency to yield $Z_{in} \approx 10Z_0 = 500\,\Omega$, Fig. 6 component values can be calculated by expanding (11) and equating it to (10), as [10, 13]:

$$\begin{aligned} R_1 &\approx Z_{in} = 500\,\Omega, \quad C_1 = \frac{1}{\Delta\omega_{1p} R_1} = 2.822\,\text{pF}, \\ L_1 &= \frac{1}{\omega_{01p}^2 C_1} = 29.493\,\text{nH}, \quad (14a) \\ R_2 &= R_1 = 500\,\Omega, \quad C_2 = \frac{1}{\Delta\omega_{3p} R_2} = 3.435\,\text{pF}, \\ L_2 &= \frac{1}{\omega_{03p}^2 C_2} = 35.907\,\text{nH}, \quad (14b) \\ R_G &= \frac{1/C_1 + 1/C_2}{\Delta\omega_{2p} + \Delta\omega_{4p} - \Delta\omega_{1p} - \Delta\omega_{3p}} = 137.3\,\Omega, \quad (14c) \\ R_F &= \frac{1}{(\omega_{02p}^2 + \omega_{04p}^2 + \Delta\omega_{2p}\Delta\omega_{4p} - \omega_{01p}^2 - \omega_{03p}^2 - \Delta\omega_{1p}\Delta\omega_{3p}) R_G C_1 C_2 - \frac{2}{R_1}} \\ &= 56.298\,\Omega, \quad (14d) \\ R_3 &= Z_0 (\Delta\omega_{6p}/\Delta\omega_{5p} - 1) = 182.08\,\Omega, \\ C_3 &= \frac{1}{\Delta\omega_{5p} R_3} = 6.738\,\text{pF}, \\ L_3 &= \frac{1}{\omega_0^2 C_3} = 15.038\,\text{nH}. \quad (14e) \end{aligned}$$

In the Fig. 5 topology, tuned frequencies of the two resonators at the op-amp input in this example are $f_{01p} = 11.0338f_c = 551.69$ MHz, and $f_{03p} = 9.0631f_c = 453.16$ MHz, and their bandwidth are $\Delta f_{1p} = 2.2561f_c = 112.81$ MHz and $\Delta f_{3p} = 1.8531f_c = 92.66$ MHz, respectively, as given by (13a). The subsequent component values are calculated by (14a) and (14b). The resonator at the op-amp output is tuned at the design center frequency, which in this example is $f_0 = 500$ MHz, and its bandwidth is $\Delta f_{5p} = 2.5946f_c = 129.73$ MHz, as given by (13c). The subsequent component values are calculated by (14e).

The Fig. 5 topology transfer function magnitude and group delay responses in this example are shown in Fig. 6, for an ideal (or buffered) source design, as well as a design with a shunt resistor $R_m = 55.55\,\Omega$ used for an approximate center-frequency impedance matching to a 50 Ω-source [13].

The center frequency NGD values for the ideal-source and resistor-matched designs are 4.47 ns and 4.35 ns, and the 3 dB-bandwidths are 100 MHz and 100.4 MHz, yielding the corresponding NGD-bandwidth products of 0.447 and 0.437, respectively.

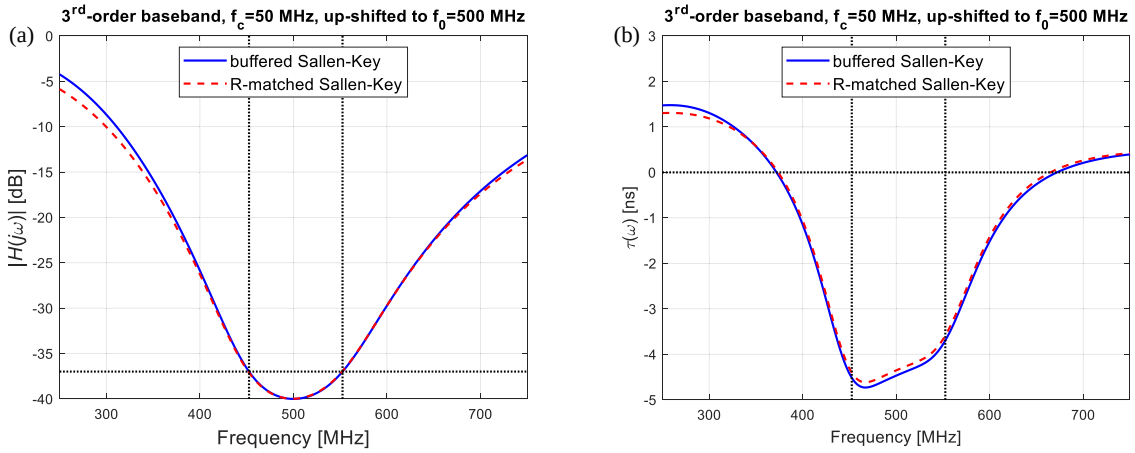

FIGURE 6. (a) Transmission coefficient and (b) group delay of the ideal source (buffered) driven Sallen-Key design, and of the shunt resistor matched design driven by a 50 Ω source, for the BSF capped reciprocal-Bessel transfer function.

The Sallen-Key topology implementation of the capped reciprocal-Bessel design presented in this paper is mostly intended as a proof-of-concept, similar to reciprocal-Butterworth and reciprocal-Chebyshev designs in [13] and [14], respectively. Further, the impact of component value variation on the transfer function characteristics in this design is somewhat smaller than the other two designs, when the sensitivity analysis described in [13] is applied. The sensitivity results are close to those presented for the passive topology discussed in the next section.

5. APPROXIMATE IMPLEMENTATION WITH PASSIVE LADDER CIRCUIT TOPOLOGY

The previous section demonstrates that a Sallen-Key topology can implement the exact BSF capped reciprocal-Bessel design transfer function, such as the one given by (10). However, since the op-amps are not in the function of amplification in this topology, the overall design has a center frequency attenuation, as evident from Fig. 6(a).

As an alternative, an all-passive resonator-based ladder topology can be employed to achieve a relatively good match to the exact BSF transfer function. An example of such ladder topology is as a π-circuit illustrated in Fig. 7, which was discussed in detail for capped reciprocal-Butterworth NGD design [13]. A T-circuit equivalent of this resonator-based topology is also discussed in [13].

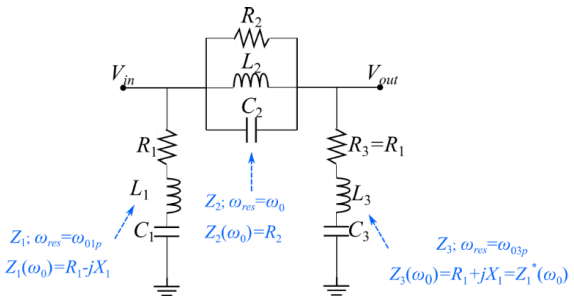

FIGURE 7. Three-resonator π-circuit ladder topology that can achieve an approximate 3rd-order baseband capped reciprocal-Bessel NGD transfer function translated to a higher center frequency ω_0 (BSF).

Transfer function of the Fig. 7 resonator-based π-circuit topology, for a given Z_0 source and load impedance, is given by [13]:

$$H(j\omega) = \frac{V_{out}}{V_{in}} = \frac{2}{\begin{array}{l}(1 + Z_2/Z_0 + Z_2/Z_3) \\ \cdot (1 + Z_0/Z_1) + (1 + Z_0/Z_3)\end{array}}. \quad (15)$$

To solve for the Fig. 7 π-circuit topology component values, transfer function (15) is first expanded with frequency-dependent impedance expressions, then factorized into three 2nd-order rational functions and equated to the capped reciprocal-Bessel BSF transfer function (10). The numerators of the two transfer functions can be exactly matched [13], such that expressions (13a)–(13c) values in this example are given by:

$$\begin{aligned}
\omega_{01p} &= \omega_{01\pi} = 11.0338\omega_c, \\
\Delta\omega_{1p} &= \Delta\omega_{1\pi} = 2.2561\omega_c, \\
\omega_{03p} &= \omega_{03\pi} = 9.0631\omega_c, \\
\Delta\omega_{3p} &= \Delta\omega_{3\pi} = 1.8531\omega_c, \\
\omega_{05p} &= \omega_{05\pi} = \omega_0 = 10\omega_c, \\
\Delta\omega_{5p} &= \Delta\omega_{5\pi} = 2.5946\omega_c.
\end{aligned} \quad (16)$$

The analysis for the π-circuit Fig. 7 topology component calculation is presented in detailed for a capped reciprocal-Butterworth design [13], and it also applies here. The analysis in [13] shows that in order to obtain the required center frequency transfer function value to be a real number and equal to the specified attenuation, $H(j\omega_0) = 1/A$, shunt impedance values Z_1 and Z_3 at ω_0 need to be complex conjugates ($R_1 = R_3$, $X_1 = -X_3$). Further, the middle resonator resistor R_2 in Fig. 7, as a function of shunt resonators parameters and the specified center frequency attenuation, is given by [13]:

$$R_2 = 2\frac{(A-1)\left(R_1^2 + X_1^2\right) - Z_0 R_1}{\left(R_1^2 + X_1^2\right)/Z_0 - 2R_1 + Z_0}. \quad (17)$$

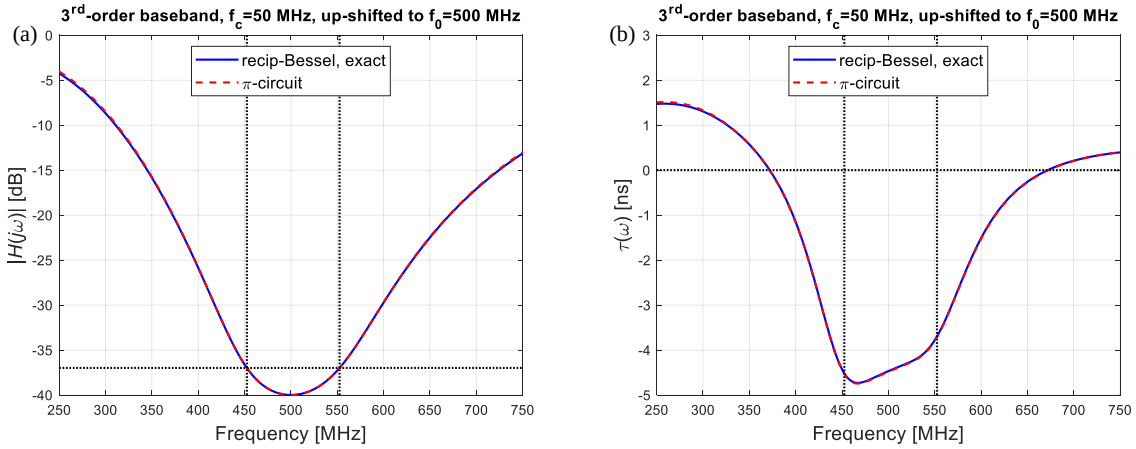

FIGURE 8. (a) Transfer function magnitude and (b) group delay responses of the exact capped reciprocal-Bessel 3rd-order design upshifted to a higher center frequency, and of the π-circuit all-passive design.

Given the described relationships between resonators component values and parameters, the only degree of freedom of this design is the shunt resonators' resistance value, R_1. An optimization based on an in-band match of transfer functions (10) and (15) can be used to determine R_1, and therefore all other component values of the π-circuit topology as well [13].

Since the prominent characteristic of any type of a Bessel filter is its in-band near-flat group delay response, the center frequency group delay curvature (2nd derivative) matching of transfer functions (10) and (15) is used to determine the optimal value $R_1 = 10.4887\,\Omega$ in this example. The π-circuit transfer function (15) denominator parameters optimized for in-band group delay curvature, compared to the exact ones in (10), are:

$$\begin{aligned} \omega_{02\pi} &= 16.4246\omega_c, \quad \Delta\omega_{2\pi} = 13.6876\omega_c, \\ \omega_{04\pi} &= 6.0884\omega_c, \quad \Delta\omega_{4\pi} = 5.0739\omega_c, \end{aligned} \tag{18a}$$

$$\begin{aligned} \omega_{02p} &= 16.2214\omega_c, \quad \Delta\omega_{2p} = 13.8211\omega_c, \\ \omega_{04p} &= 6.1647\omega_c, \quad \Delta\omega_{4p} = 5.2525\omega_c, \end{aligned} \tag{18b}$$

$$\begin{aligned} \Delta\omega_{6\pi} &= 11.8694\omega_c, \quad \Delta\omega_{6p} = 12.0432\omega_c, \\ \omega_{06\pi} &= \omega_{06p} = \omega_0 = 10\omega_c. \end{aligned} \tag{18c}$$

The design center frequency reactance magnitudes of shunt branches in Fig. 7 can be obtained from the optimized R_1 and the frequency parameters given by (16), yielding $X_1 = (1/(\omega_0 C_1) - \omega_0 L_1) = 10.1091\,\Omega$ in this example. Substituting the optimized R_1 and X_1 values into expression (17), along with $Z_0 = 50\,\Omega$ system impedance and $A = 100$ (40 dB) out-of-band gain, yields $R_2 = 544.6338\,\Omega$. All Fig. 7 component values in this example, obtained from the described optimization and expressions (16), are:

$$\begin{aligned} R_1 &= 10.4887\,\Omega, \quad L_1 = \frac{1}{\Delta\omega_{1p} R_1} = 14.799\,\text{nH}, \\ C_1 &= \frac{1}{\omega_{01p}^2 L_1} = 5.624\,\text{pF}, \end{aligned} \tag{19a}$$

$$\begin{aligned} R_3 &= 10.4887\,\Omega, \quad L_3 = \frac{1}{\Delta\omega_{3p} R_3} = 18.016\,\text{nH}, \\ C_3 &= \frac{1}{\omega_{03p}^2 L_3} = 6.847\,\text{pF}, \end{aligned} \tag{19b}$$

$$\begin{aligned} R_2 &= 544.6338\,\Omega, \quad C_2 = \frac{1}{2\omega_c R_2} = 2.253\,\text{pF}, \\ L_2 &= \frac{1}{\omega_0^2 C_2} = 44.981\,\text{nH}. \end{aligned} \tag{19c}$$

Transfer function magnitude and group delay responses of the Fig. 7 topology are shown in Fig. 8, for this example. The center frequency NGD values are 4.47 ns and 4.48 ns, for the ideal capped reciprocal-Bessel transfer function and the π-circuit design, respectively. Higher order passive ladder topology capped reciprocal-Bessel designs can be implemented by following the method described for capped reciprocal-Butterworth designs in [13].

The impact of component value variation on the transfer function characteristics in this π-circuit design is higher than the corresponding same-order classical Bessel bandpass filter. Applying the same sensitivity analysis detailed in [13], the worst-case 1% variation in the π-circuit component values yields a maximum center frequency NGD deviation of 9.3% for the capped reciprocal-Bessel design, which is less than 14.8% and 15.2% for the corresponding Butterworth and 0.5 dB-ripple Chebyshev designs, respectively. The π-circuit design presented here and those in [13, 14] are mostly intended as a proof-of-concept and are based on transfer function simulation involving ideal lumped components. To overcome challenges associated with the tuning of lumped inductance and capacitance components, microwave distributed element designs such as those presented in [25, 26] can be employed as a tunable equivalent to the π-circuit design.

6. NGD-BANDWIDTH PRODUCT ASYMPTOTIC LIMIT OF AN *N*TH-ORDER CAPPED RECIPROCAL-BESSEL DESIGN

Similar to the capped reciprocal-Butterworth [13] and capped reciprocal-Chebyshev [14] designs, the NGD-bandwidth prod-

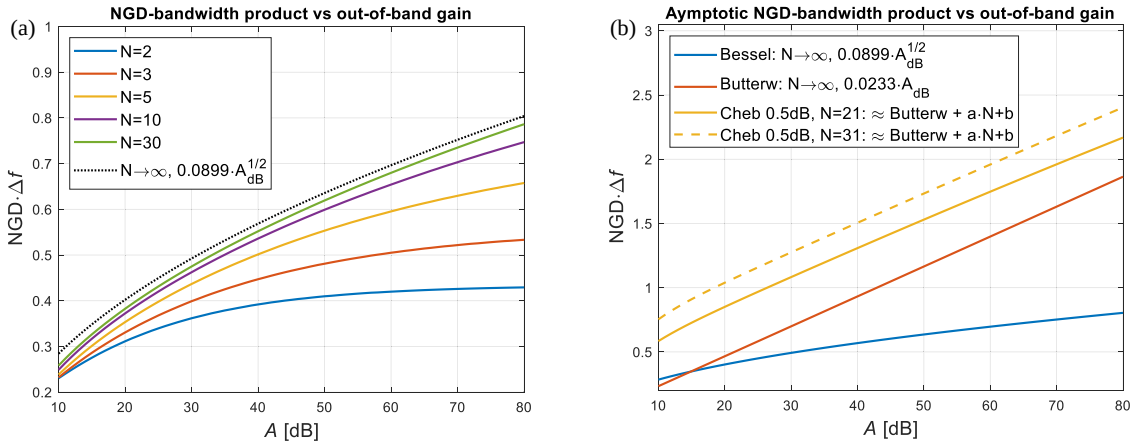

FIGURE 9. Asymptotic NGD-bandwidth product as a function of out-of-band gain for large order baseband (a) capped reciprocal-Bessel designs, and (b) comparison between capped reciprocal-Bessel, Butterworth and Chebyshev designs. Note that Chebyshev designs have an NGD-bandwidth approximately equivalent to that of a Butterworth design with an added constant offset linearly proportional to design order ($a \cdot N + b$).

uct upper asymptotic limit of a large-order capped reciprocal-Bessel design can be found as a function of the trade-off quantity, out-of-band gain.

From expression (2a), the square of the Nth-order baseband capped reciprocal-Bessel transfer function magnitude response can be approximated for a large order N by:

$$|H_N(j\omega)|^2 = \frac{a_0^2 + \left(2a_2a_0 - a_1^2\right)(j\omega)^2 + \ldots + (j\omega)^{2N}}{a_0^2 + \left(2a_2a_0 - a_1^2\right)\left(\frac{j\omega}{A^{1/N}}\right)^2 + \ldots + \left(\frac{j\omega}{A^{1/N}}\right)^{2N}} \approx \frac{\exp\left(\frac{a_1^2 - 2a_2a_0}{a_0^2}\omega^2\right)}{\exp\left(\frac{a_1^2 - 2a_2a_0}{a_0^2}\frac{\omega^2}{A^{2/N}}\right)}, \quad N \gg 1. \quad (20)$$

From (2b) it can be shown that $a_1 = a_0$, and $a_2 = a_0 \cdot (N-1)/(2N-1)$, which when being substituted into (20) yields:

$$|H_N(j\omega)| \approx \exp\left(\frac{1}{2}\frac{\omega^2}{(2N-1)}\left(1 - \frac{1}{A^{2/N}}\right)\right), \quad N \gg 1. \quad (21)$$

The 3 dB-cutoff approximation for large design order N is obtained by equating (21) to $\sqrt{2}$ and solving for frequency, which yields:

$$\omega_{c-3\,\mathrm{dB}} \approx \sqrt{\ln 2 \frac{(2N-1)}{1 - 1/A^{2/N}}}, \quad N \gg 1. \quad (22)$$

The NGD-bandwidth product is then obtained as:

$$NGD \cdot \Delta f = -\tau(0)\frac{\omega_c}{\pi} = \frac{1}{\pi}\left(1 - \frac{1}{A^{1/N}}\right)\sqrt{\frac{(2N-1)\ln 2}{1 - 1/A^{2/N}}}. \quad (23)$$

NGD-bandwidth product as the order N approaches infinity, as a function of finite out-of-band gain, becomes:

$$\lim_{N\to\infty}(NGD \cdot \Delta f) = \frac{\sqrt{\ln 2}}{\pi}\lim_{N\to\infty}\left(\frac{e^{\ln(A)/N} - 1}{\sqrt{e^{2\ln(A)/N} - 1}} \cdot \sqrt{2N-1}\right) = \frac{\sqrt{\ln 2}}{\pi}\sqrt{\ln(A)}, \quad (24)$$

or, as a function of the out-of-band gain given in decibels, $A_{\mathrm{dB}} = 20 \cdot \log(A)$, NGD-bandwidth becomes a square root asymptotic function, as also depicted in Fig. 9(a):

$$NGD \cdot \Delta f \approx \frac{1}{\pi}\sqrt{\frac{\ln 2 \cdot \ln 10}{20}}\sqrt{A_{\mathrm{dB}}} \approx 0.0899 \cdot \sqrt{A_{\mathrm{dB}}} \quad (25)$$

Expression (25) is the same square root function as the NGD-bandwidth product for cascaded identical 1st-order transfer functions discussed in [8, 13], but with the scaling parameter increased by a factor of $\sqrt{2}$. Similarly, expression (25) limit is close to the corresponding one for an engineered causal medium reported in [9] (scaling of 0.0890 vs 0.0899), which is expected since the engineered medium assumed a perfectly flat NGD within the bandwidth, with a step transition to a positive group delay in the out-of-band which then decays as $1/\omega^2$ at higher frequencies. This group delay characteristic shape of the engineered medium in [9] resembles the shape of the design presented in this paper as the design order approaches infinity, as observed in the trend of curves in Fig. 2(b). However, the design presented in this paper is based on rational transfer functions of any given order, that are more suitable for circuit implementations than the engineered medium transfer function in [9].

Asymptotic NGD-bandwidth functions of capped reciprocal-Bessel, Butterworth and Chebyshev designs are depicted in Fig. 9(b). The capped reciprocal-Butterworth design exhibits a linear asymptotic function of the out-of-band gain given in decibels [13], while capped reciprocal-Chebyshev odd-order designs exhibit approximately the same asymptotic linear function with an additional offset which is approximately a linear function of the design order, as discussed in [14].

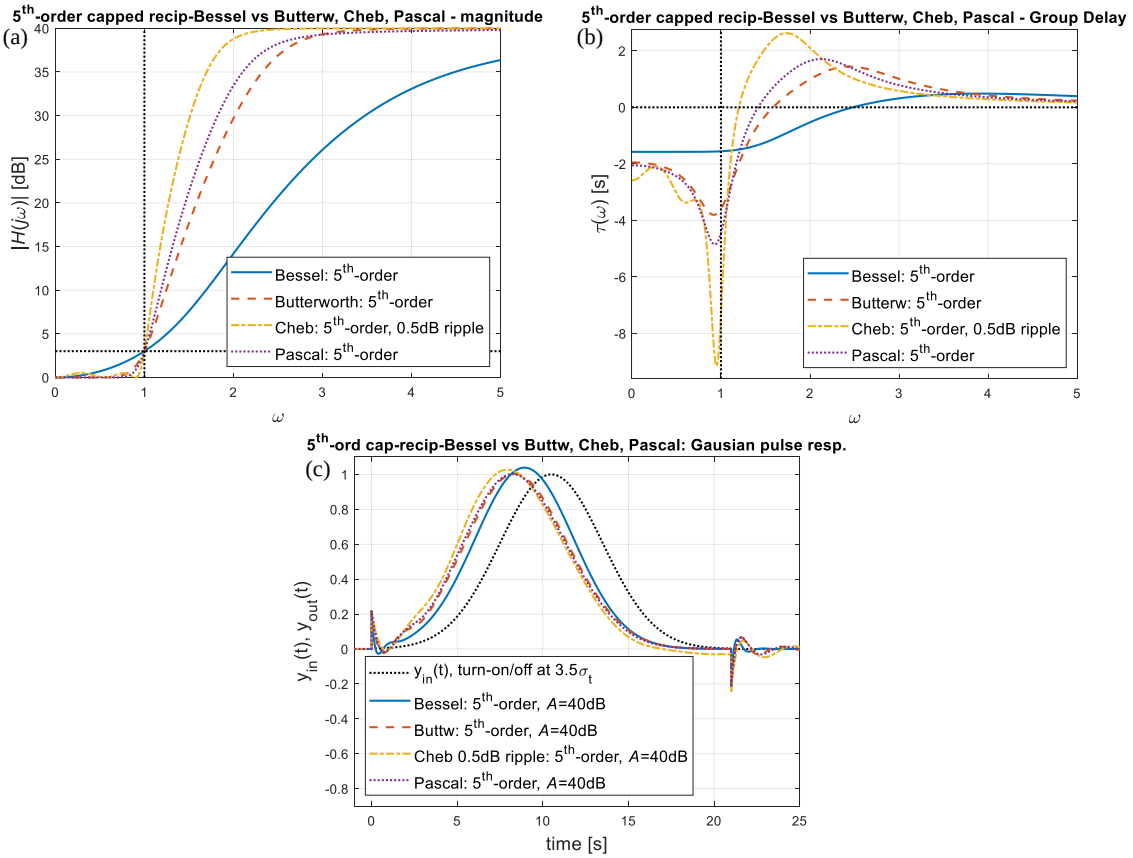

FIGURE 10. 5th-order, 40 dB out-of-band gain capped reciprocal-Bessel, Butterworth, Chebyshev (0.5 dB ripple), and Pascal baseband design's (a) magnitude, (b) group delay, and (c) time domain responses to a Gaussian pulse turned-on/off at $3.5\sigma_t$.

7. RELATIONSHIP BETWEEN TIME DOMAIN AND FREQUENCY DOMAIN NGD METRICS

As discussed in [13], the frequency domain out-of-band gain in NGD designs is proportional to the time domain transient magnitude amplification at points of discontinuity in the waveform. In this section, a Gaussian pulse waveform with finite turn-on/off times is applied to capped reciprocal-Bessel, Butterworth, Chebyshev, and Pascal NGD baseband designs. All four example designs are 5th-order, gain-compensated at the center frequency and have an out-of-band gain of $A = 100$ (40 dB), while the capped reciprocal-Chebyshev design also has a 0.5 dB in-band magnitude ripple, as captured in Fig. 10(a). The capped reciprocal-Pascal magnitude characteristic is similar to the corresponding Butterworth one, with a slightly steeper transition to the out-band, as expected from their low-pass versions [45]. As shown in Fig. 10(b), the capped reciprocal-Bessel, Butterworth, Pascal, and Chebyshev designs have center frequency NGD values of 1.575 s, 1.948 s, 2.052 s, and 2.584 s, respectively. The frequency spectrum of the chosen input Gaussian pulse has a standard deviation equal to a third of the medium 3 dB cut-off frequency, $\sigma_\omega = \omega_c/3 = 1/3$, and its turn-on/off time instances are at $3.5\sigma_t$ ($\sigma_t = 1/\sigma_\omega$) away from the peak.

The corresponding time domain pulse-peak advancement values in Fig. 10(c) are comparable at 1.575 s, 2.146 s, 2.234 s, and 2.565 s, respectively. Fig. 10(c) also shows that transient amplitudes are practically the same for the three designs, as expected due to their equal out-of-band gains [13]. Fig. 10(b) shows that out of the four designs the capped reciprocal-Bessel design has the largest bandwidth where group delay is negative, i.e., $\tau(\omega) < 0$. For all four designs, $\tau(\omega) < 0$ bandwidths approximately correspond to half of the maximum out-of-band gain decibel value, i.e., $A_{\text{dB}}/2 = 20$ dB in the chosen examples, as evident from Figs. 10(a) and 10(b).

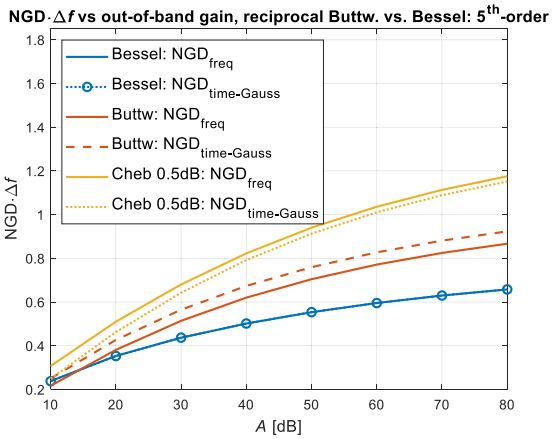

FIGURE 11. NGD-bandwidth product (using 3 dB-bandwidth) as a function of out-of-band gain for 5th-order capped reciprocal-Bessel, Butterworth and Chebyshev designs determined using frequency domain NGD and time domain NGD for an applied Gaussian pulse.

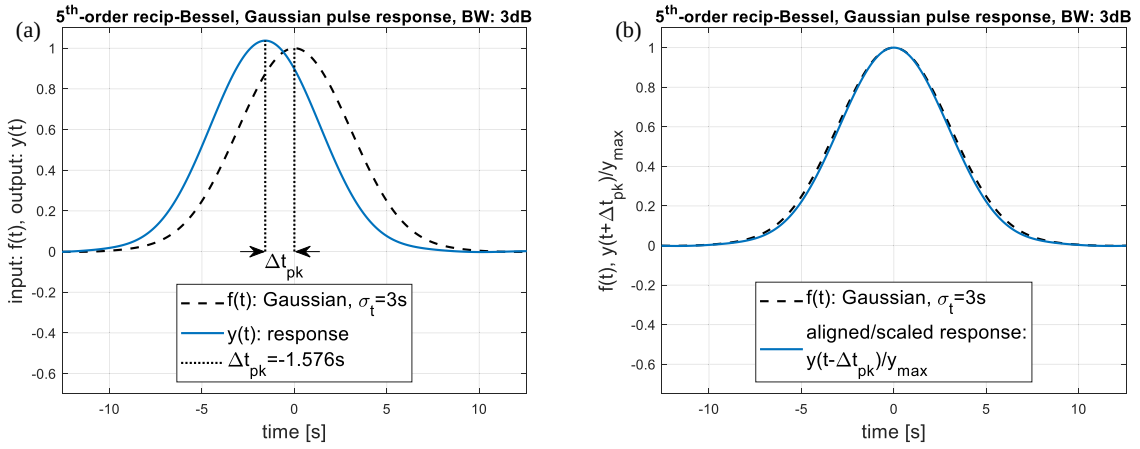

FIGURE 12. (a) Input Gaussian pulse with a frequency spectrum cut-off at $\omega_c = 1$, and the corresponding output waveform for a 5th-order capped reciprocal-Bessel gain-compensated design. (b) The same comparison but with the output waveform shifted by Δt_{pk} and normalized by $|y(t)|_{\max}$.

Figure 11 shows NGD-bandwidth product (using 3 dB-bandwidth) as a function of the out-of-band gain for 5th-order capped reciprocal-Bessel, Butterworth, and Chebyshev designs. Fig. 11 shows the plots based on both the center frequency NGD and time domain NGD values corresponding to time-advancement of a Gaussian pulse peak. It is evident that for the capped reciprocal-Bessel design the frequency and time domain NGD values are practically equal due to a near-flat group delay within the 3 dB-bandwidth. On the other hand, Fig. 11 shows that for the capped reciprocal-Butterworth design the observed time domain NGD (Gaussian pulse peak advancement) is higher than the corresponding center frequency NGD. This phenomenon is attributed to the capped reciprocal-Butterworth design group delay response increasing in magnitude away from the center frequency towards the band edges, as shown in Fig. 10(b). Conversely, Fig. 11 shows that for the capped reciprocal-Chebyshev design the observed time domain NGD is somewhat lower than the corresponding center frequency NGD.

8. IN-BAND COMBINED MAGNITUDE/PHASE RESPONSE DISTORTION METRIC

Various Figure of Merit (FOM) metrics can be used to assess and compare performances of different NGD designs. The FOM reported in [10, 13, 14] is given as a ratio of the achieved center frequency NGD-bandwidth product, and the trade-off quantity, out-of-band gain:

$$FOM = \frac{NGD \cdot BW}{A_{\text{dB}}}. \tag{26}$$

As demonstrated in Section 7, and discussed in [8–10, 13, 14], an undesired property of the out-of-band gain is amplification of transients associated with discontinuous waveforms, such as those with finite turn-on/off times. For NGD application with no concerns about transients, the performance focus may be on the gain-compensation of the center frequency attenuation. In that case $1/A_{\text{dB}}$ term in expression (26) can be replaced by the NGD design's center frequency magnitude response value, $|H(j\omega_0)|$.

Like any other medium, NGD designs introduce distortion to propagated waveforms, caused by variations in the magnitude and group delay responses (phase non-linearity) within the frequency in-band (typically defined by 3 dB-bandwidth). The combined magnitude/phase in-band distortion affects not only continuous waveforms, but also the "steady-state" part of waveforms that contain transients [13].

The observed output waveform distortion is a function of not only the medium's transfer function (in-band magnitude/phase distortion), but also the input waveform's frequency spectrum. A distortion metric proposed in [13, 14] for an NGD baseband design with a transfer function $H(j\omega)$ and a 3 dB-bandwidth cut-off ω_c, an input waveform with frequency spectrum $F(j\omega)$, output waveform peak advancement Δt_{pk}, and the input/output pulse peak values $f_{\max}/y_{\max}$, is given by:

$$D_{in\text{-}band} = \sqrt{\frac{\int_0^{\omega_c} \left|F(j\omega) - e^{-j\omega\Delta t_{pk}} F(j\omega)H(j\omega) \cdot f_{\max}/y_{\max}\right|^2 d\omega}{\int_0^{\omega_c} |F(j\omega)|^2 \, d\omega}}. \tag{27}$$

As an example, the distortion metric expression (27) is calculated for an input Gaussian pulse with 6 standard deviations of its frequency spectrum fitting within the NGD medium's 3 dB-bandwidth. This waveform is applied to a 5th-order capped reciprocal-Bessel design with $A = 40$ dB out-of-band gain, and input/output waveforms are captured in Fig. 12. The calculated distortion metric is $D_{\text{in-band-Gaussian}} = 0.0319$. As a reference, application of the same waveform to a classical 1st-order low-pass filter with a matching 3 dB-bandwidth yields a higher value of the distortion metric, $D_{\text{low-pass-Gaussian}} = 0.0411$.

For selected 5th-order capped reciprocal-Bessel and capped reciprocal-Butterworth designs, NGD-bandwidth product as a function of out-of-band gain is shown in Figs. 13(a) and (b), using time domain observed NGD (pulse peak advancement) for Gaussian and sinc input waveforms, respectively. Solid curves in Figs. 13(a) and (b) correspond to 3 dB-bandwidths when calculating the product, while dashed and dotted curves

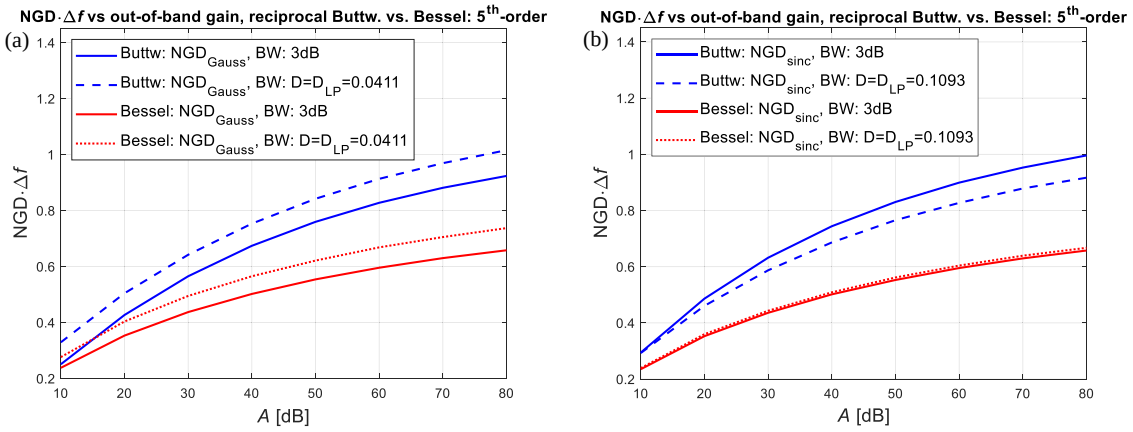

FIGURE 13. NGD-bandwidth product (using time domain NGD) for (a) Gaussian and (b) sinc input waveforms applied to selected 5th-order designs with 3 dB-bandwidth (solid curves) vs. bandwidth yielding the same distortion metric as a 1st-order low-pass filter ($D_{LP} = 0.0411$, 0.1093 for Gaussian and sinc pulses, respectively).

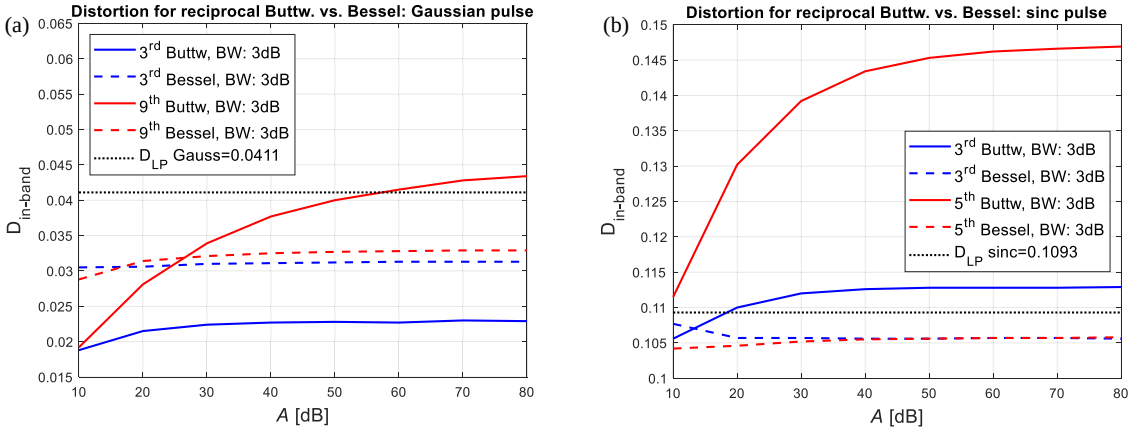

FIGURE 14. Distortion metric values for (a) Gaussian and (b) sinc input waveforms applied to selected capped reciprocal-Bessel and capped reciprocal-Butterworth designs with 3 dB-bandwidth.

correspond to bandwidths needed to equal the distortion metric values of the chosen reference 1st-order low-pass filter ($D = 0.0411$ for a Gaussian pulse and $D = 0.1093$ for a sinc waveform).

For both considered designs, the distortion metric for a Gaussian pulse is lower than a sinc pulse due to its frequency spectrum tapering off towards the band edges and therefore reducing the effects of the medium's amplitude/phase variations. Thus, as indicated in Fig. 13(a), the bandwidth can be increased past the 3 dB cut-off for a Gaussian pulse input to adhere to the reference distortion value, resulting in higher NGD-bandwidth product (dashed and dotted) curves. Conversely, for a sinc pulse input, which has a flat in-band frequency spectrum and therefore doesn't reduce the effects of the medium's amplitude/phase variations, the bandwidth of the capped reciprocal-Butterworth design needs to be reduced below the 3 dB cut-off to adhere to the reference distortion value, as evident from a lower NGD-bandwidth (dashed) curve in Fig. 13(b). The capped reciprocal-Bessel design is not affected as much due to medium's lower in-band amplitude/phase variations, as evident from its still slightly higher NGD-bandwidth (dotted) curve in Fig. 13(b).

For capped reciprocal-Bessel and capped reciprocal-Butterworth designs of selected orders and a fixed 3 dB-bandwidth, the in-band distortion metric values obtained from (27) are shown in Figs. 14(a) and (b), for Gaussian and sinc waveforms, respectively. For a Gaussian pulse input, Fig. 14(a) shows that it takes a 9th-order (or higher) capped reciprocal-Butterworth design to start reaching the reference distortion value of a 1st-order low-pass filter, $D_{\text{Gauss}} = 0.0411$. On the other hand, Fig. 14(b) shows that for a sinc input it takes only a 3rd-order capped reciprocal-Butterworth design to start reaching the reference distortion value, $D_{\text{sinc}} = 0.1093$. For both input waveforms, dashed curves in Figs. 14(a) and (b) demonstrate that the considered capped reciprocal-Bessel designs stay below the respective reference distortion values due to the discussed medium's low amplitude/phase variations.

Further, the distortion metric values are virtually constant for capped reciprocal-Bessel designs of different orders and out-of-band gains, as evident from Figs. 14(a) and 14(b). This is a result of the amplitude and group delay in-band characteristics of the capped reciprocal-Bessel designs not changing much with the design order or out-of-band gain, as evident from Figs. 2 and 3.

TABLE 2. NGD performance metrics for selected Nth-order capped reciprocal-Bessel baseband designs with 3 dB-bandwidth, compared to capped reciprocal-Butterworth, Chebyshev, and Pascal designs.

Design order/ filter type	Out-of-band gain, A [dB]	NGD-BW product, $-\tau(0) \cdot \Delta f_{3\,\mathrm{dB}}$	FOM [1/dB]	$\Delta t_{pk} \cdot \Delta f_{3\,\mathrm{dB}}$ (Gaussian)	Distortion: $D_{\text{in-band}}$ (Gaussian) $D_{\text{ref}} = 0.0411$	$\Delta t_{pk} \cdot \Delta f_{3\,\mathrm{dB}}$ (sinc)	Distortion: $D_{\text{in-band}}$ (sinc) $D_{\text{ref}} = 0.1093$
3rd-order, Bessel	40	0.4470	0.0112	0.4464	$0.76 \times D_{\text{ref}}$	0.4440	$0.97 \times D_{\text{ref}}$
3rd-order, Butterworth	40	0.4995	0.0125	0.5416	$0.55 \times D_{\text{ref}}$	0.5800	$1.03 \times D_{\text{ref}}$
3rd-order, Pascal	40	0.5220	0.0130	0.5632	$0.58 \times D_{\text{ref}}$	0.6136	$1.11 \times D_{\text{ref}}$
3rd-order, Cheb 0.5 dB	40	0.6192	0.0155	0.6016	$0.63 \times D_{\text{ref}}$	0.6648	$1.31 \times D_{\text{ref}}$
5th-order, Bessel	40	0.5014	0.0125	0.5016	$0.78 \times D_{\text{ref}}$	0.5016	$0.97 \times D_{\text{ref}}$
5th-order, Butterworth	40	0.6200	0.0155	0.6736	$0.69 \times D_{\text{ref}}$	0.7440	$1.31 \times D_{\text{ref}}$
5th-order, Pascal	40	0.6531	0.0163	0.7112	$0.75 \times D_{\text{ref}}$	0.7960	$1.54 \times D_{\text{ref}}$
5th-order, Cheb 0.5 dB	40	0.8226	0.0206	0.7920	$1.01 \times D_{\text{ref}}$	0.9008	$2.06 \times D_{\text{ref}}$
7th-order, Bessel	40	0.5226	0.0131	0.5224	$0.79 \times D_{\text{ref}}$	0.5224	$0.97 \times D_{\text{ref}}$
7th-order, Butterworth	40	0.6896	0.0172	0.7528	$0.81 \times D_{\text{ref}}$	0.8448	$1.63 \times D_{\text{ref}}$
7th-order, Pascal	40	0.7188	0.0180	0.7888	$0.90 \times D_{\text{ref}}$	0.8976	$1.96 \times D_{\text{ref}}$
7th-order, Cheb 0.5 dB	40	0.9404	0.0235	0.8928	$1.32 \times D_{\text{ref}}$	1.0352	$2.76 \times D_{\text{ref}}$

Table 2 summarizes a performance comparison of the proposed capped reciprocal-Bessel design against the capped reciprocal-Butterworth design from [13], the capped reciprocal-Chebyshev (in this case with a 0.5 dB in-band ripple) design from [14], and the capped reciprocal-Pascal design, for selected design orders and out-of-band gain. The table shows the achieved center frequency NGD-bandwidth product (using 3 dB-bandwidth) and the resulting Figure-of-Merit (FOM) accounting for the trade-off out-of-band gain. Further, the table shows time domain NGD (for Gaussian and sinc pulses), and the associated distortion metric values relative to the reference 1st-order low-pass filter distortion for the same waveforms. For a given waveform, Table 2 shows that the distortion metric values are virtually constant for capped reciprocal-Bessel designs, while the values increase significantly with the design order for capped reciprocal-Butterworth, Pascal, and Chebyshev designs, and eventually surpass the capped reciprocal-Bessel design values (at 3rd-order for a sinc, and 7th-order for a Gaussian pulse). On the other hand, the capped reciprocal-Chebyshev, Butterworth, and Pascal designs achieve a higher NGD-bandwidth product than the capped reciprocal-Bessel design.

As discussed in [10, 13, 14], in many publications the wider $\tau(\omega) < 0$ bandwidth where the group delay is negative is used in metrics instead of the 3 dB-bandwidth, resulting in a seemingly better performance. This comes at the expense of a higher distortion for wideband input waveforms, for any NGD design with an out-of-band gain higher than approximately 6 dB, and therefore more than 3 dB variation within the $\tau(\omega) < 0$ bandwidth.

An alternative distortion metric to the one given by (27) is based on input/output waveform cross-correlation [32, 36], and it approximately yields values that are a square root of $1 - D^2$. Another NGD medium distortion metric which considers both amplitude and group delay variation (phase non-linearity) is presented in [39], with the main difference to expression (27) being that it does not factor the specific applied waveform into the distortion.

Aiming to keep an NGD design's distortion metric such as (27) low, assume that input/output waveform fidelity is desired. Alternatively, when magnitude/phase (group delay) equalization is the objective of an NGD application, the distortion metric of the cascaded design including both the equalizing and preceding stage(s) can be evaluated to assess the performance.

9. CONCLUSION

The prototype baseband NGD filter introduced in this paper is based on a reciprocal transfer function of a classical Bessel low-pass filter, multiplied by a "capping" classical Bessel filter transfer function of the same order but with a larger bandwidth (capped reciprocal-Bessel design). Similar to the capped reciprocal-Butterworth [13] and capped reciprocal-Chebyshev [14] designs which are based on two transfer function ratios of their respective classical low-pass filters, it was shown that the presented baseband capped reciprocal-Bessel design can be translated to a finite-attenuation band-stop filter (BSF) centered at a non-zero center frequency. It was further shown that the resulting capped reciprocal-Bessel BSF design can be implemented via resonator-based Sallen-Key topology, or all-passive ladder topologies, similar to designs in [13, 14].

The prototype capped reciprocal-Bessel design was shown to achieve an NGD-bandwidth product that in the upper asymptotic limit (design order approaches infinity) is the same square root function of the out-of-band gain in decibels associated with the distributed medium with cascaded identical 1st-order baseband NGD stages [8, 13], but with a higher proportionality factor. This proportional factor of the square root asymptotic function is close to that one of the engineered flat in-band NGD characteristic causal medium presented in [9], as expected given the group delay flatness property of the capped reciprocal-Bessel design presented here.

The very flat in-band group delay also makes the proposed capped reciprocal-Bessel transfer function suitable for constant phase shifter implementations [17, 18], which are used in phased array antenna applications.

The performance of the proposed capped reciprocal-Bessel design is also evaluated for an in-band combined magnitude/phase distortion metric discussed in [10, 13, 14], for applied Gaussian and sinc waveforms. It was shown for higher order designs that the distortion metric for the proposed design is virtually constant and generally lower than the distortion metric of the corresponding capped reciprocal-Butterworth [13], capped reciprocal-Chebyshev [14], and capped-reciprocal Pascal designs, when 3 dB-bandwidth designs are considered. On the other hand, the capped reciprocal-Chebyshev, Butterworth, and Pascal designs achieve a higher NGD-bandwidth product.

REFERENCES

[1] Mojahedi, M., E. Schamiloglu, F. Hegeler, and K. J. Malloy, "Time-domain detection of superluminal group velocity for single microwave pulses," *Physical Review E*, Vol. 62, No. 4, 5758, 2000.

[2] Wang, Y., Y. Zhang, L. He, F. Liu, H. Li, and H. Chen, "Direct observation of negative phase velocity and positive group velocity in time domain for composite right/left-handed transmission lines," *Journal of Applied Physics*, Vol. 100, No. 11, 113503, 2006.

[3] Ibraheem, I. A., J. Schoebel, and M. Koch, "Group delay characteristics in coplanar waveguide left-handed media," *Journal of Applied Physics*, Vol. 103, No. 2, 024903, 2008.

[4] Brillouin, L., *Wave Propagation and Group Velocity*, Academic Press, New York, 2013.

[5] Mojahedi, M., K. J. Malloy, G. V. Eleftheriades, J. Woodley, and R. Y. Chiao, "Abnormal wave propagation in passive media," *IEEE Journal of Selected Topics in Quantum Electronics*, Vol. 9, No. 1, 30–39, 2003.

[6] Stenner, M. D., D. J. Gauthier, and M. A. Neifeld, "Fast causal information transmission in a medium with a slow group velocity," *Physical Review Letters*, Vol. 94, No. 5, 053902, 2005.

[7] Bolda, E. L., R. Y. Chiao, and J. C. Garrison, "Two theorems for the group velocity in dispersive media," *Physical Review A*, Vol. 48, No. 5, 3890, Nov. 1993.

[8] Kandic, M. and G. E. Bridges, "Asymptotic limits of negative group delay in active resonator-based distributed circuits," *IEEE Transactions on Circuits and Systems I: Regular Papers*, Vol. 58, No. 8, 1727–1735, Aug. 2011.

[9] Kandic, M. and G. E. Bridges, "Limits of negative group delay phenomenon in linear causal media," *Progress In Electromagnetics Research*, Vol. 134, 227–246, 2013.

[10] Kandic, M. and G. E. Bridges, "Negative group delay prototype filter based on cascaded second order stages implemented with Sallen-Key topology," *Progress In Electromagnetics Research B*, Vol. 94, 1–18, 2021.

[11] Solli, D., R. Y. Chiao, and J. M. Hickmann, "Superluminal effects and negative group delays in electronics, and their applications," *Physical Review E*, Vol. 66, No. 5, 056601, 2002.

[12] Dorrah, A. H. and M. Mojahedi, "Nonanalytic pulse discontinuities as carriers of information," *Physical Review A*, Vol. 93, No. 1, 013823, 2016.

[13] Kandic, M. and G. E. Bridges, "Negative group delay prototype filter based on the reciprocal transfer function of a low-pass Butterworth filter capped at finite out-of-band gain," *Progress In Electromagnetics Research B*, Vol. 106, 17–38, 2024.

[14] Kandic, M. and G. E. Bridges, "Negative group delay prototype filter based on the ratio of two classical Chebyshev filter transfer functions," *Progress In Electromagnetics Research B*, Vol. 107, 139–153, 2024.

[15] Macke, B., B. Ségard, and F. Wielonsky, "Optimal superluminal systems," *Physical Review E*, Vol. 72, No. 3, 035601(R), Sep. 2005.

[16] Macke, B. and B. Ségard, "Propagation of light-pulses at a negative group-velocity," *The European Physical Journal D — Atomic, Molecular, Optical and Plasma Physics*, Vol. 23, 125–141, 2003.

[17] Ravelo, B., M. L. Roy, and A. Pérennec, "Application of negative group delay active circuits to the design of broadband and constant phase shifters," *Microwave and Optical Technology Letters*, Vol. 50, No. 12, 3078–3080, 2008.

[18] Meng, Y., Z. Wang, S.-J. Fang, and H. Liu, "Broadband phase shifter with constant phase based on negative group delay circuit," *Progress In Electromagnetics Research Letters*, Vol. 103, 161–169, 2022.

[19] Ravelo, B., "Similitude between the NGD function and filter gain behaviours," *International Journal of Circuit Theory and Applications*, Vol. 42, No. 10, 1016–1032, 2014.

[20] Lucyszyn, S., I. D. Robertson, and A. H. Aghvami, "Negative group delay synthesiser," *Electronics Letters*, Vol. 29, No. 9, 798–800, Apr. 1993.

[21] Nakanishi, T., K. Sugiyama, and M. Kitano, "Demonstration of negative group delays in a simple electronic circuit," *American Journal of Physics*, Vol. 70, No. 11, 1117–1121, Nov. 2002.

[22] Kitano, M., T. Nakanishi, and K. Sugiyama, "Negative group delay and superluminal propagation: An electronic circuit approach," *IEEE Journal of Selected Topics in Quantum Electronics*, Vol. 9, No. 1, 43–51, Jan.-Feb. 2003.

[23] Siddiqui, O. F., M. Mojahedi, and G. V. Eleftheriades, "Periodically loaded transmission line with effective negative refractive index and negative group velocity," *IEEE Transactions on Antennas and Propagation*, Vol. 51, No. 10, 2619–2625, Oct. 2003.

[24] Ravelo, B., A. Perennec, M. L. Roy, and Y. G. Boucher, "Active microwave circuit with negative group delay," *IEEE Microwave and Wireless Components Letters*, Vol. 17, No. 12, 861–863, Dec. 2007.

[25] Choi, H., Y. Jeong, C. D. Kim, and J. S. Kenney, "Bandwidth enhancement of an analog feedback amplifier by employing a negative group delay circuit," *Progress In Electromagnetics Research*, Vol. 105, 253–272, 2010.

[26] Choi, H., Y. Jeong, C. D. Kim, and J. S. Kenney, "Efficiency enhancement of feedforward amplifiers by employing a negative group-delay circuit," *IEEE Transactions on Microwave Theory and Techniques*, Vol. 58, No. 5, 1116–1125, May 2010.

[27] Mirzaei, H. and G. V. Eleftheriades, "Realizing non-Foster reactive elements using negative-group-delay networks," *IEEE Transactions on Microwave Theory and Techniques*, Vol. 61, No. 12, 4322–4332, Dec. 2013.

[28] Chaudhary, G., Y. Jeong, and J. Lim, "Microstrip line negative group delay filters for microwave circuits," *IEEE Transactions on Microwave Theory and Techniques*, Vol. 62, No. 2, 234–243, Feb. 2014.

[29] Wu, C.-T. M. and T. Itoh, "Maximally flat negative group-delay circuit: A microwave transversal filter approach," *IEEE Transactions on Microwave Theory and Techniques*, Vol. 62, No. 6, 1330–1342, Jun. 2014.

[30] Wu, Y., H. Wang, Z. Zhuang, Y. Liu, Q. Xue, and A. A. Kishk, "A novel arbitrary terminated unequal coupler with bandwidth-enhanced positive and negative group delay characteristics," *IEEE Transactions on Microwave Theory and Techniques*, Vol. 66, No. 5, 2170–2184, 2018.

[31] Wan, F., N. Li, B. Ravelo, and J. Ge, "O=O shape low-loss negative group delay microstrip circuit," *IEEE Transactions on Circuits and Systems II: Express Briefs*, Vol. 67, No. 10, 1795–1799, Oct. 2019.

[32] Ravelo, B., F. Wan, and J. Ge, "Anticipating actuator arbitrary action with a low-pass negative group delay function," *IEEE Transactions on Industrial Electronics*, Vol. 68, No. 1, 694–702, Jan. 2021.

[33] Wang, Z., S. Zhao, H. Liu, and S. Fang, "A compact dual-band differential negative group delay circuit with wideband common mode suppression," *IEEE Journal of Microwaves*, Vol. 2, No. 4, 720–725, Oct. 2022.

[34] Nair, R. G. and S. Natarajamani, "Design theory of compact power divider with reconfigurable power division and negative group delay characteristics," *Scientific Reports*, Vol. 13, No. 1, 7222, May 2023.

[35] Palson, C. L., D. D. Krishna, and B. R. Jose, "Planar tunable negative group delay circuit with low reflection loss," *Progress In Electromagnetics Research Letters*, Vol. 113, 53–59, 2023.

[36] Ravelo, B., H. Bilal, S. Rakotonandrasana, M. Guerin, F. Haddad, S. Ngoho, and W. Rahajandraibe, "Transient characterization of new low-pass negative group delay RC-network," *IEEE Transactions on Circuits and Systems II: Express Briefs*, Vol. 71, No. 1, 126–130, Jan. 2024.

[37] Zhang, A., J. Xu, and Z. Liu, "A microstrip linear-phase BPF using dual-band negative group delay equalizers," *IEEE Microwave and Wireless Technology Letters*, Vol. 34, No. 4, 387–390, Apr. 2024.

[38] Chang, N., A. Yuan, Y. Wang, and J. Liu, "Multi-band pass negative group delay circuit with low insertion loss," *International Journal of Circuit Theory and Applications*, Jul. 2024.

[39] Nako, J., C. Psychalinos, A. S. Elwakil, and B. J. Maundy, "A note on the bandwidth of negative group delay filters," *International Journal of Circuit Theory and Applications*, 2024.

[40] Nako, J., C. Psychalinos, B. J. Maundy, and A. S. Elwakil, "Elementary negative group delay filter functions," *Circuits, Systems, and Signal Processing*, Vol. 43, No. 6, 3396–3409, 2024.

[41] Maundy, B. J., A. S. Elwakil, and C. Psychalinos, "Systematic design of negative group delay circuits," *AEU — International Journal of Electronics and Communications*, Vol. 174, 155060, 2024.

[42] Nako, J., C. Psychalinos, A. S. Elwakil, and B. J. Maundy, "Power-law negative group delay filters," *Electronics*, Vol. 13, No. 3, 522, 2024.

[43] United States Patent Office (USPTO) application number: 18/491922.

[44] United States Patent Office (USPTO) application number: 19/017634.

[45] Goodman, T. J. and M. F. Aburdene, "Pascal filters," *IEEE Transactions on Circuits and Systems I: Regular Papers*, Vol. 55, No. 10, 3090–3094, Nov. 2008.